CENP-A and topoisomerase-II antagonistically affect chromosome length

A.-M. Ladouceur,[1]* Rajesh Ranjan,[3]* Lydia Smith,[2] Tanner Fadero,[1] Jennifer Heppert,[1] Bob Goldstein,[1] Amy Shaub Maddox,[1] and Paul S. Maddox[1]

[1]Department of Biology and [2]Department of Genetics, University of North Carolina at Chapel Hill, Chapel Hill, NC
[3]Department of Biology, Johns Hopkins University, Baltimore, MD

The size of mitotic chromosomes is coordinated with cell size in a manner dependent on nuclear trafficking. In this study, we conducted an RNA interference screen of the *Caenorhabditis elegans* nucleome in a strain carrying an exceptionally long chromosome and identified the centromere-specific histone H3 variant CENP-A and the DNA decatenizing enzyme topoisomerase-II (topo-II) as candidate modulators of chromosome size. In the holocentric organism *C. elegans*, CENP-A is positioned periodically along the entire length of chromosomes, and in mitosis, these genomic regions come together linearly to form the base of kinetochores. We show that CENP-A protein levels decreased through development coinciding with chromosome-size scaling. Partial loss of CENP-A protein resulted in shorter mitotic chromosomes, consistent with a role in setting chromosome length. Conversely, topo-II levels were unchanged through early development, and partial topo-II depletion led to longer chromosomes. Topo-II localized to the perimeter of mitotic chromosomes, excluded from the centromere regions, and depletion of topo-II did not change CENP-A levels. We propose that self-assembly of centromeric chromatin into an extended linear array promotes elongation of the chromosome, whereas topo-II promotes chromosome-length shortening.

Introduction

During early development, mitotic chromosome size scales to cell size; repeated cell division in the absence of embryo growth reduces cell size, and concomitantly, chromosome size decreases (Kieserman and Heald, 2011; Hara et al., 2013; Ladouceur et al., 2015). Chromosome size scaling is critical for life, as a single mitotic chromosome in an early embryo can be as large as the entire metaphase plate of smaller cells late in development (unpublished data). Previously, nuclear transport via the Ras-related nuclear protein (RAN) pathway was shown to play an important role in regulating mitotic chromosome size, implicating nuclear proteins in chromosome-size regulation (Hara et al., 2013; Ladouceur et al., 2015). To find proteins whose nuclear localization is critical for mitotic chromosome scaling, we devised and executed an RNAi screen of the *Caenorhabditis elegans* nucleome in a sensitized setting.

We performed our screen in a *C. elegans* strain that harbors an exceptionally long chromosome as the result of a telomere fusion event between the two longest chromosomes (5 and X; Lowden et al., 2008, 2011). This strain is viable in laboratory conditions and contains a genome size not significantly different from the wild-type parent strain. We predicted that depletions with a robust effect on chromosome length would lead to embryonic lethality in our long-chromosome strain but not in control animals. This strategy identified the centromere-specific histone H3 variant CENP-A (HCP-3/CPAR-1 in *C. elegans*, hereafter CENP-A) and topoisomerase-II (TOP-2 in *C. elegans*, hereafter topo-II), among 13 other proteins, as being required for viability in the presence of an exceptionally long chromosome (Fig. 1, a and b).

CENP-A–containing nucleosomes define centromeres and make up an estimated 2–5% of the metazoan genome. In *C. elegans*, as well as many other organisms, centromeres are not restricted to a single region of each chromosome, resulting in CENP-A dispersed along each chromosome (holocentric; Maddox et al., 2006; De Rop et al., 2012). Current hypotheses in both monocentric (regionalized) and holocentric organisms predict that patches of CENP-A chromatin assemble to form a unified centromeric chromatin region in mitosis (Blower et al., 2002). The mechanism of mitotic centromere assembly is unknown; however, CENP-A nucleosomes have increased internal rigidity that could potentially drive self-assembly on the outer face of mitotic chromosomes forming a linear array. In agreement with this hypothesis, in vitro reconstitution of synthetic arrays showed that CENP-A–containing nucleosomes are more condensed than

*A.-M. Ladouceur and R. Ranjan contributed equally to this paper.

Correspondence to Paul S. Maddox: pmaddox@unc.edu

Abbreviations used: dsRNA, double-stranded RNA; NEBD, nuclear envelope breakdown; NGM, nematode growth medium; RAN, Ras-related nuclear protein; sfGFP, superfolded GFP; SIM, structured illumination microscopy.

The Rockefeller University Press
J. Cell Biol. Vol. 216 No. 9 2645–2655
https://doi.org/10.1083/jcb.201608084

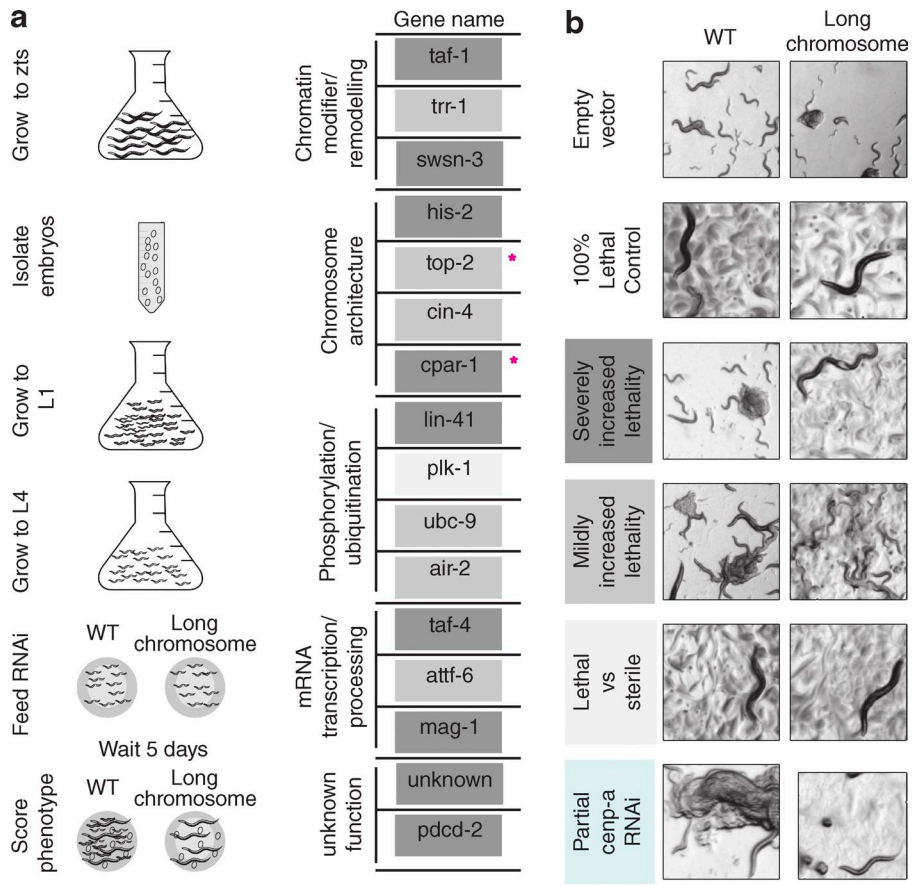

Figure 1. **RNAi screen of the *C. elegans* nucleome identifies chromosomal architecture proteins as regulators of chromosome size.** (a) Diagrammatic flow and list of positive hits from the RNAi screen. Pink asterisks highlight potential regulators of chromosome length tested in this study. zts, zygotes. (b) Representative images of five different phenotypes and partial CENP-A RNAi observed after RNAi treatment of wild-type or long-chromosome strains.

bulk chromatin (Panchenko et al., 2011; Geiss et al., 2014). In *C. elegans*, CENP-A depletion results in each chromosome collapsing into a ball rather than forming rod-shaped chromosomes during mitosis, supporting the idea that CENP-A chromatin stretches are structurally important (Maddox et al., 2006). Here, we find, counterintuitively to our screen, that CENP-A chromatin levels positively correlate with chromosome length; lower levels of CENP-A lead to shorter chromosomes (see Results and discussion).

Topo-II is involved in numerous DNA metabolic processes through its enzymatic activity: DNA decatenation of loops (Nitiss, 2009). Topo-II localizes to the central long axis of monocentric mitotic chromosomes (Earnshaw et al., 1985; Gasser et al., 1986), and loss of topo-II function impairs chromosome assembly, leading to chromosome segregation defects in most eukaryotic cells (Uemura et al., 1987; Adachi et al., 1991; Hirano and Mitchison, 1993). In addition to mitotic errors, topo-II loss of function activates the G2 checkpoint and leads to decreased transcriptional activity (Downes et al., 1994; Mondal and Parvin, 2001). The *C. elegans* early embryo has weak checkpoint activity and is transcriptionally silent, allowing cell-cycle progression after topo-II depletion (Budirahardja and Gönczy, 2009). We find that topo-II levels are constant through early development, and it localizes spatially independent of CENP-A. Depletion of topo-II led to abnormally long chromosomes, consistent with a recent study in vertebrate cells (Farr et al., 2014).

In sum, our screen designed to identify proteins and required to limit chromosome length identified proteins that contribute to both shortening and lengthening of chromosomes. Our evidence supports the idea that CENP-A and topo-II localize and function independently to provide structure and to determine the length of holocentric mitotic chromosomes.

Results and discussion

A reverse genetic screen for proteins required to segregate an abnormally long chromosome

To identify proteins required for setting chromosome length, we individually RNAi depleted a subset (~400) of proteins predicted to localize to the *C. elegans* nucleus in two conditions: a strain harboring a chromosomal fusion between 5 and X and the control parent strain (wild type; Lowden et al., 2008, 2011). Compared with wild-type *C. elegans*, our long-chromosome strain has the same genome size and indistinguishable viability in laboratory conditions (Lowden et al., 2008, 2011). To perform the screen, L4-stage larvae were incubated with individual clones from a library of bacteria expressing double-stranded RNAs (dsRNAs) targeting the nucleome (Fig. 1 a; Tursun et al., 2011). The viability of RNAi-treated progeny was scored 5 d later, and a range of phenotypes was recorded (Fig. 1 b). Our strategy identified 15 individually confirmed nuclear proteins as required for embryogenesis in our long-chromosome strain. The list includes chromatin modifiers (*taf-1*, *trr-1*, and *swsn-3*), chromosome architecture (*his-2*, *top-2*, *cin-4*, and *cpar-1*), and phosphorylation/ubiquitination (*lin-41*, *plk-1*, *ubc-9*, and *air-2*), as well as several with unknown function (*taf-4*, *attf-6*, *mag-1*, and *pdcd-2*). One of the 15 hits, Aurora-B (*air-2*), has been shown to be required for shortening an extra-long chromosome during budding yeast anaphase (Neurohr et

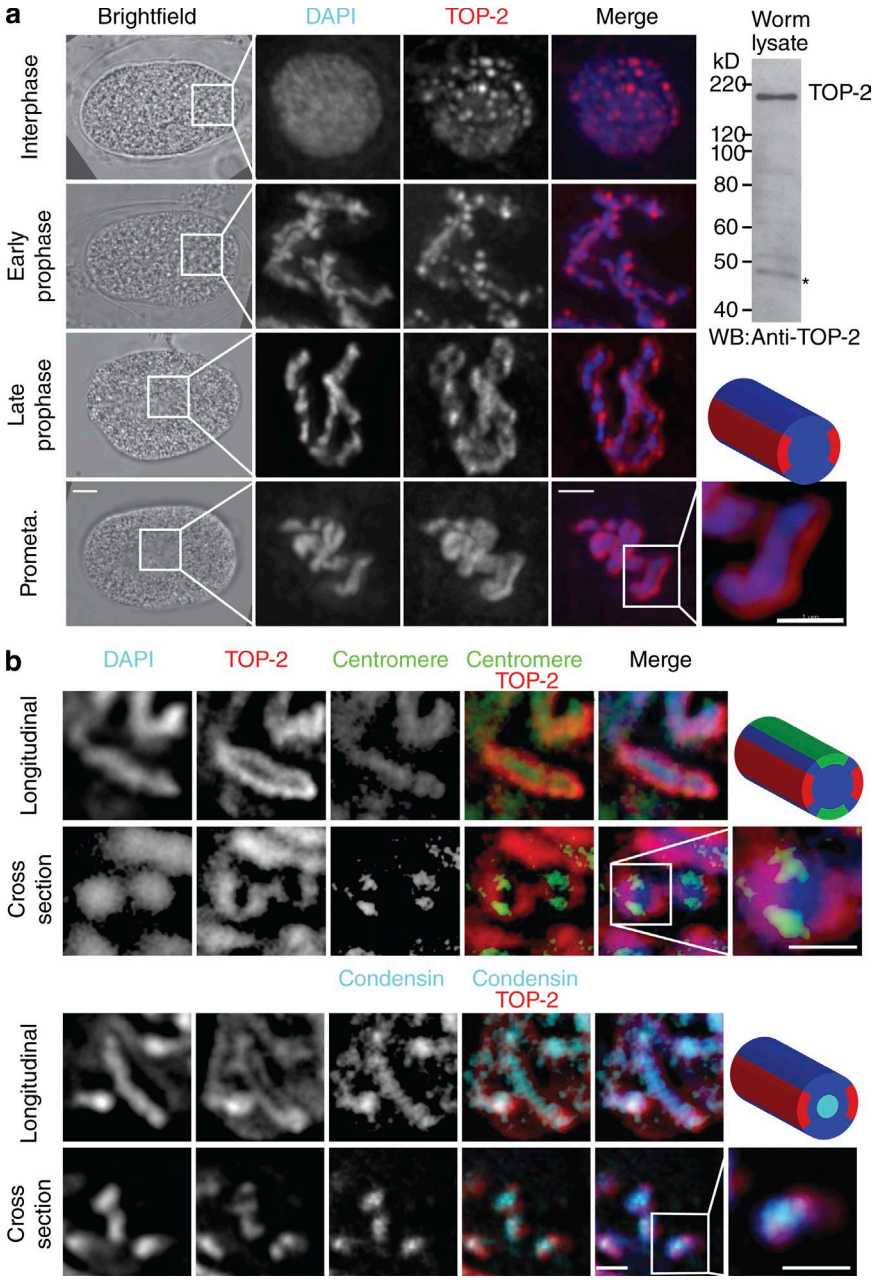

Figure 2. **Endogenous topo-II forms axes distinct from the centromere and the condensin complex.** (a) One-cell embryos fixed and stained with anti–topo-II antibody and DAPI, at different mitotic stages. The insets show zoomed-in images of a single prometaphase (Prometa.) chromosome. Anti–topo-II antibody probing the whole-worm lysate by Western blotting (WB) is shown. The asterisk indicates a band that is unaffected by top-2 RNAi. (b) Centromeres marked with GFP–KNL-2 (OD31) or GFP-condensin (GFP–CAPG-2 and OD112) expressing single-cell embryos immunostained with anti–topo-II antibody to compare centromere and condensin with topo-II localization. The montage shows longitudinal views of a single prometaphase chromosome (first and third rows) and cross-sectional views of a chromosome (second and last rows). Insets show a zoomed-in cross-sectional view of a single chromosome. Schematics of a single prometaphase chromosome show a 3D view of spatial organization of topo-II (red), centromere (green), condensin (light blue), and DNA (dark blue). Bars: (fluorescence images) 1 µm; (brightfield images) 5 µm.

al., 2011), revealing that our strategy identified proteins that impact chromosome size.

Among our hits, two proteins previously reported as required for chromosome condensation and segregation in *C. elegans* stood out: CENP-A and topo-II (Fig. 1, a and b; Maddox et al., 2006; Bembenek et al., 2013). *C. elegans* uniquely expresses two orthologues of CENP-A; HCP-3 is the dominant form required for mitosis, whereas CPAR-1 has no known function in embryos (Monen et al., 2015). Because these orthologues share extensive DNA sequence identity, it is not possible to independently target them by RNAi; therefore, we will refer to their depletion as CENP-A RNAi (Monen et al., 2005, 2015). Topo-II also has two *C. elegans* orthologues (CIN-4 and TOP-2, both hits in our screen). However, the TOP-2 gene harbors the most extensive homology and, thus, was used in our studies. Long-chromosome embryos treated with partial CENP-A or topo-II RNAi (mimicking the levels from the screen) arrested with varying numbers of cells and appeared to exhibit chromosome loss independent of cell lineage or fate (Fig. S1, a–c). Thus, reducing the levels of CENP-A (and thus centromere chromatin) or topo-II resulted in lethality in *C. elegans* long-chromosome embryos compared with wild type.

Endogenous CENP-A and topo-II localize to distinct linear areas on mitotic holocentric chromosomes

Consistent with a structural role in chromosome condensation, CENP-A localizes linearly along mitotic chromosomes in *C. elegans*. However, topo-II localization has not previously been evaluated (Buchwitz et al., 1999). In monocentric organisms (e.g., mammals), topo-II localizes to chromosome arms and is concentrated at the condensed centromere regions, leading to the hypothesis that it serves as a structural element (Earnshaw et al., 1985; Taagepera et al., 1993; Rattner et al., 1996; Warsi et al.,

2008). To test whether topo-II localized in a manner consistent with it serving as a structural element on *C. elegans* holocentric chromosomes, we generated an affinity-purified polyclonal antibody directed against *C. elegans* topo-II. Immunofluorescence staining with this antibody revealed linear localization along the exterior of mitotic chromosomes after nuclear envelope breakdown (NEBD; prometaphase; Fig. 2 a). The linear, exterior localization pattern is unlikely caused by a failure of the antibody to penetrate the chromatin, as other similarly generated antibodies can penetrate chromosomes prepared with identical methods (Oegema et al., 2001). Localization was lost after complete RNAi of topo-II, confirming that our RNAi is effective and the antibody specific (Fig. S1, d and e). Topo-II localization was confirmed using an endogenous superfolded GFP (sfGFP)–tagged version (the only copy in the animal, generated by genome editing; Fig. S2, a–c; Dickinson and Goldstein, 2016).

To further evaluate the roles of topo-II and CENP-A, we sought to determine whether topo-II localizes to chromosomes in a manner distinct from the centromere, which also forms a linear, exterior axis (Buchwitz et al., 1999). We fixed and stained embryos for CENP-A and topo-II and found that topo-II was excluded from centromeres (Fig. 2 b). These data support the hypothesis that topo-II and CENP-A are independent. The condensin complex localizes to and is required for assembly of mitotic chromosomes. In *C. elegans*, condensin localizes to a linear element on mitotic chromosomes. We costained topo-II and condensin (the SMC-4 subunit) and found distinct localization on mitotic chromosomes (Fig. 2 b). Thus, based on high-resolution analysis, topo-II localizes distinctly from CENP-A and the condensin complex on holocentric mitotic chromosomes.

CENP-A and topo-II contribute to chromosome length in opposing manners

Our screen suggested that CENP-A and topo-II contribute to setting proper chromosome length in some fashion. We predicted that depleting either protein would affect chromosome size in wild-type animals. Depletion (48 h RNAi) of either protein in *C. elegans* with wild-type chromosome length resulted in embryonic lethality stemming from zygotic condensation and segregation defects that preclude analysis of chromosome-length scaling during embryogenesis (Maddox et al., 2006). To characterize the cytological effects underlying the lethality observed in our screen, we partially depleted these proteins and analyzed single-cell embryos (Fig. 3 a and Table 2). We measured chromosome length and found that partial depletion of CENP-A resulted in shorter chromosomes compared with controls (Fig. 3 b and Table 1). In contrast, depletion of topo-II resulted in longer chromosomes (Figs. 3 b and S2 d and Table 1).

To dissect this functional interplay, we partially depleted CENP-A and topo-II simultaneously (Fig. 3 b). Double depletion rescued chromosome length in the early embryos nearly to control conditions (statistically different from each individual RNAi, Fig. 3 b and Table 1; and depletion quantification, Table 2). These animals displayed severe anaphase bridging defects (Fig. 3 b), indicating that the proteins were in fact depleted to a significant level. These findings suggest that CENP-A–containing chromatin elongates, whereas topo-II compacts holocentric chromosomes. Given that our screen was designed to identify proteins that promote chromosome shortening (as we have found topo-II to do), it was unexpected to find that CENP-A promotes chromosome elongation. We conclude that our screen was not as specific as intended and that hits can be thought of more broadly as involved in mitotic chromosome structure. It is not unheard of for two proteins with opposing functions to reveal similar cellular phenotypes (for instance, Rho GTPase-activating protein [GAP] or guanine exchange factor [GEF] depletion leads to failure of cytokinesis; unpublished data).

Table 1. **Mean chromosome length measurements at the one-cell stage**

Condition	Chromosome length
	µm
Control RNAi	3.7 ± 0.08
Partial CENP-A RNAi	**2.81 ± 0.062**
Partial topo-II RNAi	**4.95 ± 0.12**
Double CENP-A/topo-II RNAi	*3.39 ± 0.08*

Chromosome lengths in bold are significantly different from the control with $P < 0.0001$. For lengths in italic, $P < 0.001$. The double RNAi is significantly different from each single RNAi.

Table 2. **Mean chromatin CENP-A fluorescence intensity at the one-cell stage relative to control**

Condition	CENP-A fluorescence intensity relative to control
Control RNAi	87.18% ± 4.19
CENP-A RNAi	**–0.68% ± 0.51**
Partial CENP-A RNAi	**21.26% ± 3.34**
Partial topo-II RNAi	76.8% ± 3.06
Double CENP-A/topo-II RNAi	**3.83% ± 2.58**
rcc-1 RNAi	*71.53% ± 3.19*
Double CENP-A/rcc-1 RNAi	**21.93% ± 1.53**

Intensities in bold are significantly different from control with $P < 0.0001$. For intensities in italic, $P < 0.05$.

Titration of CENP-A, but not topo-II, via nuclear trafficking is required for chromosome-size scaling during embryonic development

Previously, we showed that nuclear trafficking via the RAN pathway is required for regulating chromosome-size scaling in the *C. elegans* early embryo. We proposed a model wherein a chromosome compaction inhibitor is titrated inside the nucleus over the course of development (concomitant with reduced nuclear size), resulting in reduced chromosome length in smaller cells (Ladouceur et al., 2015). To test this hypothesis, we measured chromatin-associated CENP-A protein levels just after NEBD during various stages of early embryonic development. CENP-A chromatin levels decreased during development from the two- to eight-cell stage (Fig. 4 a; two- to eight-cell stage, $P < 0.0001$ [one-way ANOVA]; 16-cell stage and older, $P = 0.3113$ [one-way ANOVA]). This decrease essentially matched the rate of chromosome-size scaling that we reported previously (Ladouceur et al., 2015). In contrast, topo-II levels on chromatin did not vary during embryonic development until after the 50-cell stage, and depletion of topo-II did not affect CENP-A protein levels (Fig. S2 e; 2- to 49-cell stage, $P = 0.5720$ [one-way ANOVA]; 50-cell stage and older, $P < 0.0001$ [one-way ANOVA]; and Fig. 2 a and Table 2).

Based on the above results, we hypothesized that partial depletion of the RanGEF RCC1 would disrupt CENP-A import (Ladouceur et al., 2015). Depletion of RCC1 led to reduced levels of CENP-A on chromatin that remained constant over

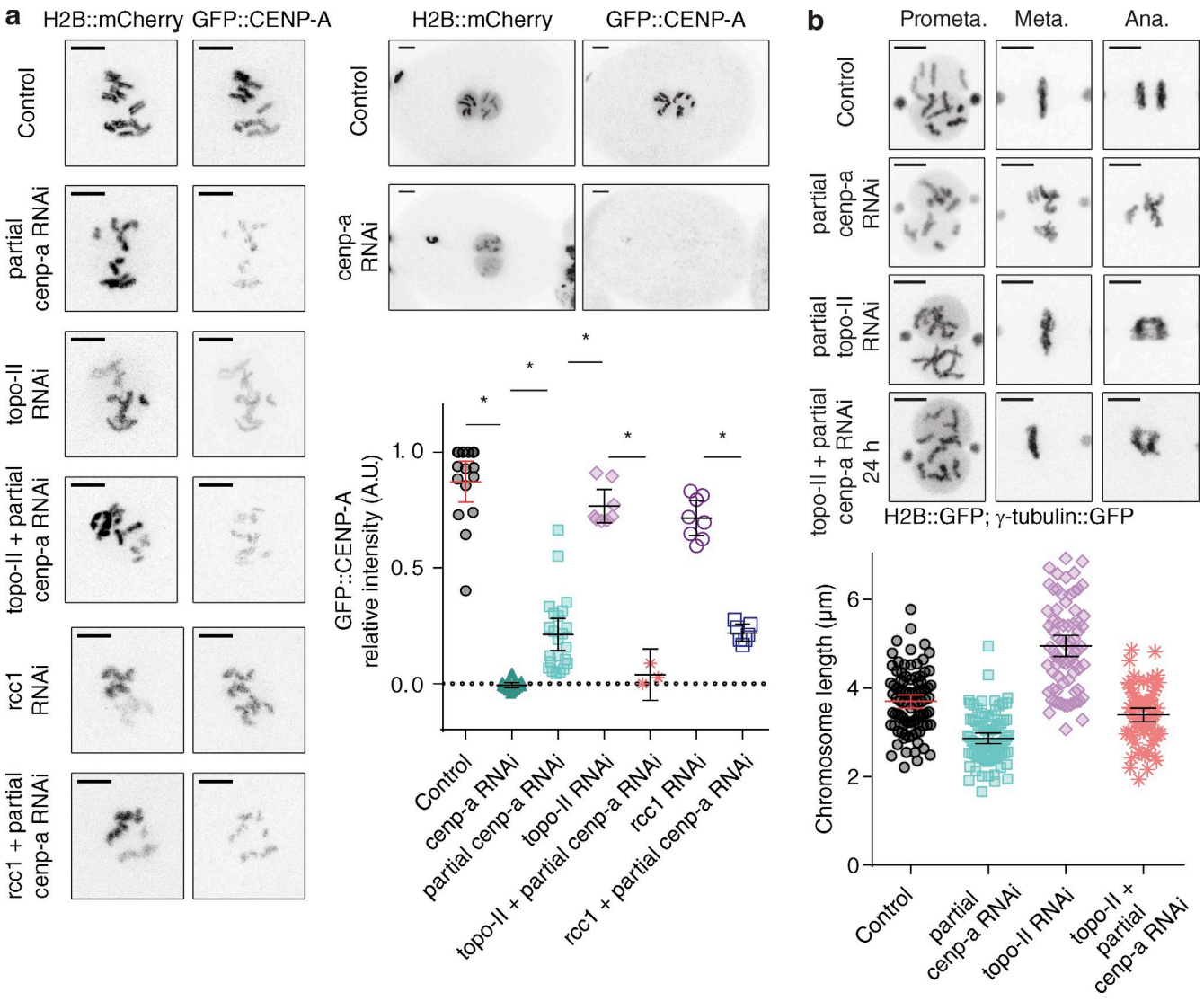

Figure 3. **CENP-A and topo-II work antagonistically to set chromosome size.** (a) Representative images of single-cell embryos expressing H2B::mCherry and GFP::CENP-A (strain OD421; Fig. S2; Gassmann et al., 2012) and measurements of GFP::CENP-A intensity frequency distribution in control (black circle; *n* = 16), CENP-A RNAi (dark green triangles; *n* = 17), partial CENP-A RNAi (aqua squares; *n* = 23), topo-II RNAi (purple diamonds; *n* = 8), topo-II + partial CENP-A RNAi (pink stars; *n* = 3), rcc-1 (open purple circle; *n* = 8), or rcc1 + partial CENP-A RNAi (open blue squares; *n* = 7) conditions. Asterisks denote statistically different pairwise comparisons (see Table 2 for details). (b) Representative images of TH32 (animals of normal karyotype [six haploid chromosomes]) single-cell embryos containing GFP::histone-H2B (to visualize chromosomes) and GFP::γ-tubulin (centrosomes; to monitor mitotic progression) and frequency distribution of chromosome length measurements after control (black circles; *n* = 89), partial CENP-A RNAi (aqua squares; *n* = 84), topo-II RNAi (purple diamonds; n = 75), or topo-II + partial CENP-A RNAi (pink stars; *n* = 71). Ana., anaphase; Meta, metaphase; Prometa., prometaphase. Conditions are significantly different by one-way ANOVA. Error bars represent 95% confidence interval. Bars, 5 µm.

the course of early development, compared with the control (Fig. 4 b; control, $P < 0.0001$ [one-way ANOVA]; RCC1 RNAi, P = NS [one-way ANOVA]). Double RCC1/CENP-A partial RNAi led to chromosome length not significantly different from each single RNAi (Fig. S2 f). In all cases, CENP-A levels scaled with chromosome size. However, we cannot exclude that other RAN pathway targets are critical to setting mitotic chromosome size. To test whether CENP-A import or CENP-A chromatin assembly is necessary for chromosome-length scaling, we blocked CENP-A nucleosome assembly, but not nuclear import, by depleting the centromere licensing factor KNL-2 (Maddox et al., 2007). Partial KNL-2 depletion (full depletion is lethal) reduced CENP-A chromatin without affecting CENP-A protein levels, concomitantly increasing unincorporated nuclear CENP-A (Fig. S1 c). Chromosomes in embryos partially depleted of KNL-2 were abnormally short, fitting with our data that CENP-A chromatin leads to longer chromosomes (Fig. S1 c). Together, these results support the idea that CENP-A chromatin is required for chromosome-length scaling during early *C. elegans* development.

CENP-A acts as a ruler for chromosome length

In *C. elegans*, CENP-A is incorporated and maintained in discrete domains distributed periodically along the genomic positional length of each chromosome (Oegema et al., 2001; Gassmann et al., 2012; Steiner and Henikoff, 2014). Because of this discontinuous distribution, CENP-A chromatin appears, via high-resolution light microscopy, as a patchy plate on the surface of metaphase holocentric chromosomes. CENP-A

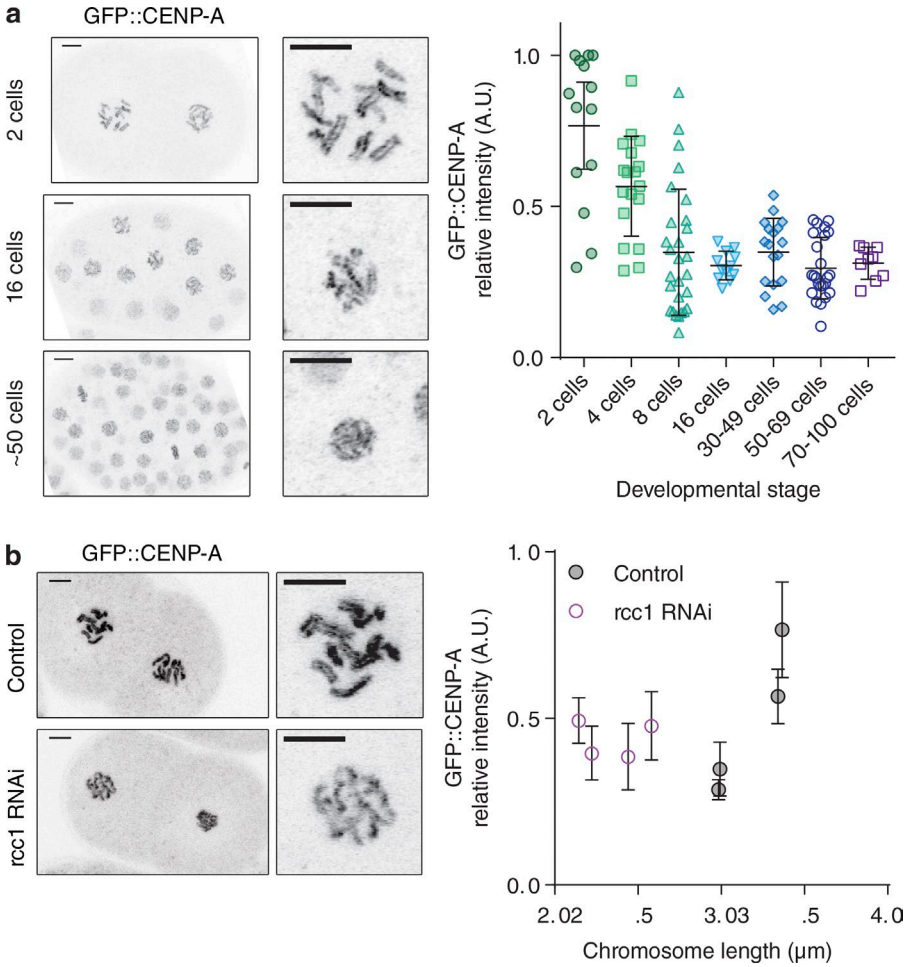

Figure 4. **Chromatin-associated CENP-A levels decrease during development and are regulated by nuclear import.** (a) Representative images of embryos expressing GFP::CENP-A at three different developmental stages and frequency distribution of relative intensity measurements of chromatin GFP::CENP-A during development, from the 2- to 100-cell stage. Relative intensity measurements of chromatin GFP::CENP-A during development are different by one-way ANOVA. *n* =14 (2 cells), 18 (4 cells), 28 (8 cells), 12 (16 cells), 18 (30–49 cells), 24 (50–69 cells), and 9 (70–100 cells). Error bars represent mean and 95% confidence interval. (b) Representative images of two cell–stage embryos expressing GFP::CENP-A (OD421) after RNAi depletion of control (black circles; *n* = 72) or rcc-1 RNAi (purple circles; *n* = 68). Mean GFP::CENP-A relative intensities according to chromosome length are graphed (mean chromosome length measurements at 2-, 4-, 8-, and 16-cell stages taken from Ladouceur et al., 2015. Control conditions are different by one-way ANOVA ($P < 0.001$), and rcc1 RNAi conditions are not different by one-way ANOVA ($P = 0.14$). Bars, 5 µm.

chromatin assembles during prophase to form a linear array on each chromosome, perhaps contributing to the rigidity of mitotic chromosomes (Maddox et al., 2006). In support of this idea, severe loss of CENP-A chromatin causes chromosomes to appear collapsed and round, instead of rod shaped (Oegema et al., 2001; Maddox et al., 2006). As a partial decrease of CENP-A chromatin resulted in abnormally short but still rod-shaped chromosomes, we hypothesized that mitotic self-association of dispersed CENP-A–containing chromosome loci contributes to chromosome morphology, with the quantity of centromeric DNA acting as a molecular ruler that sets chromosome length. To test this hypothesis, we plotted the amount of CENP-A on each fully condensed mitotic chromosome just before metaphase relative to chromosome length (Fig. 5, a and b). We found a linear relation between CENP-A levels and chromosome length, with shorter chromosomes containing less CENP-A than longer chromosomes (Fig. 5 b; control: $y = 7.405 x \pm 0.5 + 3.49 \pm 3.49$). This effect is mediated by centromeric chromatin, as depletion of the kinetochore protein CENP-C (whose depletion does not affect CENP-A levels in *C. elegans*) did not alter chromosome length (Maddox et al., 2007). By extension, this analysis reveals that the amount of CENP-A per unit length of condensed chromosome (not genetic distance) is constant in *C. elegans*.

If CENP-A epigenetic domains indeed set mitotic chromosome size, changing the amount of CENP-A chromatin should modify the ruler. In *C. elegans* embryos, CENP-A incorporation is inversely correlated to germline transcription (high transcription, low CENP-A incorporation; low transcription, high CENP-A; Gassmann et al., 2012; Steiner and Henikoff, 2014). We disrupted germline transcription by depleting the Argonaut protein CSR-1 (Claycomb et al., 2009) and thus increased the total amount of CENP-A incorporated in individual chromosomes in early embryos (Fig. 5 b). CENP-A overincorporation led to mitotic errors in the first division, precluding analysis in the resulting blastomeres. Interestingly, the linear relation between CENP-A chromatin levels and chromosome length was altered in CENP-A overincorporation in single-cell embryos (Fig. 5 b; control: $y = 7.405 x \pm 0.5 + 3.49 \pm 3.49$; csr-1 RNAi: $y = 15.82 x \pm 1.68 - 1.80 \pm 12.92$; differences in slope, $P < 0.0001$). These results are consistent with the hypothesis of an upper limit, or plateau, for chromosome length as reported for other mitotic structures (Schubert and Oud, 1997; Wühr et al., 2008; Ladouceur et al., 2015). In cells depleted of CSR-1, CENP-A was overincorporated compared with controls at the same developmental stage. As expected from a CENP-A ruler model, cells with increased CENP-A had longer chromosomes than controls (Fig. 5 b).

Centromere domain size, rather than domain number, defines *C. elegans* mitotic chromosome length

Chromatin immunoprecipitation sequencing analysis in *C. elegans* found that CENP-A localizes in broad chromatin domains with each chromosome possessing ~100 domains spaced at distances ranging from 290 bp to 1.9 Mb (median of 83 kb),

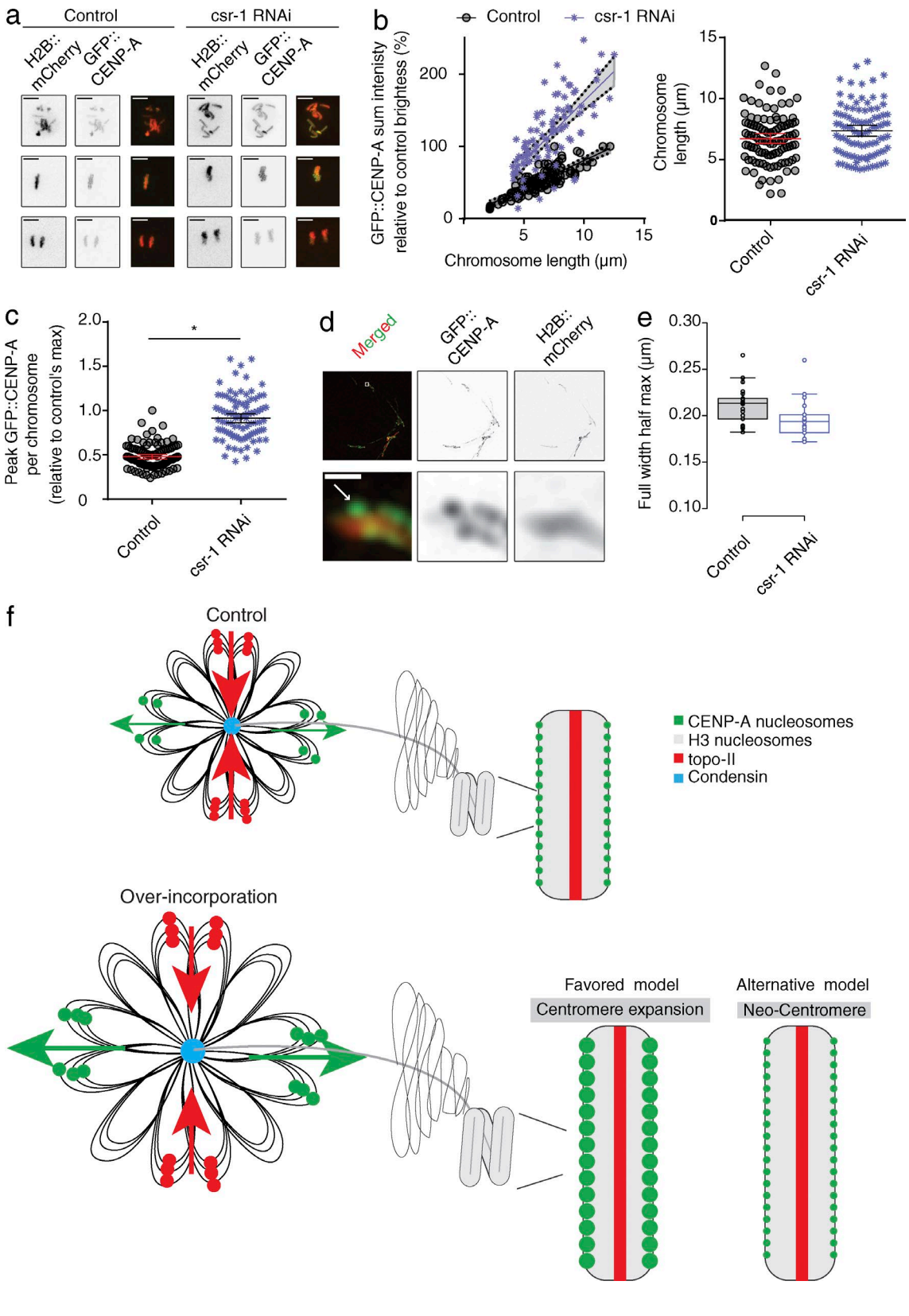

Figure 5. **The amount of CENP-A incorporated into existing centromere domains sets the chromosome length.** (a) Representative images of single-cell embryos expressing GFP::CENP-A and H2B::mCherry after control or CSR-1 RNAi. (b) GFP::CENP-A sum intensity for each individual segmented chromosome in relation to chromosome length and chromosome length for individual segmented chromosomes after control and csr-1 RNAi. Each slope is statistically different from zero. The slopes of the linear regression of the two conditions are statistically different. $P < 0.01$. (c) GFP::CENP-A maximum voxel intensity of individual chromosomes after control and CSR-1 RNAi. (b and c) All intensity values are relative to the maximum intensity of controls. Control (black circles), $n = 104$; and csr-1 RNAi (purple stars), $n = 94$ chromosomes measured in >10 embryos. (d) Representative SIM images of chromatin squashes of a single-cell GFP::CENP-A embryo after control RNAi. The arrow points to a representative focus measured in e. (e) Distribution plot of full-width

a distance that roughly fits the predicted loop size formed in mitotic chromosome assembly (Naumova et al., 2013; Steiner and Henikoff, 2014). In light of our measurements of decreased CENP-A levels throughout development, we developed two hypothesis: (1) either the number of CENP-A nucleosomes in each centromeric domain is larger in longer chromosomes (centromere expansion hypothesis) or (2) number of domains decreases over developmental time resulting in proportionally shorter chromosomes in smaller cells (neo-centromere hypothesis; Fig. 5 f). In the first case, individual, subresolution CENP-A domains would have an increased intensity in longer chromosomes, whereas in the second, individual domains would retain their intensity, but there would be more domains per chromosome in longer chromosomes. We measured CENP-A intensity of individual resolvable domains in conditions that resulted in altered CENP-A amounts (CSR-1 RNAi). We found an increase in CENP-A maximum fluorescent intensity per domain on individually segmented chromosomes in CSR-1 RNAi compared with control embryos (Fig. 5 c; control: 0.48 ± 0.01; CENP-A overincorporation: 0.91 ± 0.03). These results support the centromere expansion hypothesis for CENP-A loading.

CENP-A domains observed in the microscope do not represent bead-on-a-string level of chromatin and are more likely to be regions of GFP::CENP-A chromatin of a few kilobases or longer. To more precisely analyze individual domains, we performed prometaphase chromosomes squashes by squashing individually observed embryos (Fig. 5, d and e). We were unable to detect changes in CENP-A foci size or distribution per unit length of chromatin by confocal microscopy (not depicted) or structured illumination microscopy (SIM; Fig. S3 a; Gustafsson et al., 1999), which effectively doubles spatial resolution. We found that CENP-A features have the same size in control cells and CSR-1 RNAi, suggesting those domains are diffraction limited (Fig. 5, d and e; and Fig. S3 b). Therefore, our data support the hypothesis that CENP-A nucleosome levels are modulated within predefined regions as opposed to CENP-A being ectopically deposited in normally noncentromeric loci.

The study of mitotic chromosomes has a rich history, including the observation in 1912 by Conklin of developmentally coupled chromosome-size scaling (Conklin, 1912). Here, we show that, in the holocentric organism *C. elegans*, centromere size is a determining factor in chromosome size. Our data affect two aspects in chromosome biology: chromosome-size scaling and centromeric chromatin structure. Unstructurally, holocentromeres are nearly identical to monocentromeres. Our findings that CENP-A amount defines the centromere, and thus chromosome length in *C. elegans*, raise the possibility that the same is true in monocentric conditions. In human cells, CENP-A levels can be reduced significantly without disrupting mitotic function (Black et al., 2007); mitotic kinetochore size has not been addressed in this case because centromeres are subresolution. It will be interesting to test in the future whether CENP-A levels impact kinetochore size (tri-laminar plate) or solely centromeric chromatin size in human cells.

Recently, genomic techniques (3C derivatives and chromatin immunoprecipitation sequencing) have emerged allowing the detection of intrachromosomal chromatin interactions that generate loops on mitotic chromosomes (Belton et al., 2012; Mizuguchi et al., 2014; Eagen et al., 2015). We propose that mitotic centromeric chromatin assembles an exterior axis with internal, noncentromeric chromatin looped to the chromosome body. We found that topo-II can act to constrain chromosome length, which we further propose acts via modulating chromatin loops. Specifically, centromeric chromatin energetically prefers to assemble into a thin line that would result in a lower loop density, possibly through a surfactant (i.e., an electrostatic charge barrier)-based mechanism as recently proposed for Ki-67 (Cuylen et al., 2016). Thus, these antagonizing forces lead to a structurally sound, linear mitotic chromosome in *C. elegans*.

Materials and methods

Antibodies and antibody labeling

A C-terminal fragment consisting of amino acids 1,350–1,470 from recombinant *C. elegans* topo-II was amplified with the primers 5′-GCG CGCCCATGGATGTTCGATTCGGACGATGAC-3′ and 5′-GCGCGC CTCGAGTCATCTTGGAGCCACAACGAAGC-3′. This fragment was inserted into a bacterial expression vector (pGEX; GE Life Sciences) and expressed in *Escherichia coli* cells. Purified protein was used for antibody production in rabbit (Institute for Research in Immunology and Cancer core facility). Topo-II antibodies were immunopurified using the same fragment fused to a his tag using standard technologies. A fraction of topo-II and CENP-A antibodies was labeled with DyLight 499 and 649 (DyLight Microscale Labeling kit; Thermo Fisher Scientific). Antibodies were used at concentrations of 10 and 0.33 µg/ml for immunofluorescence and Western blotting, respectively.

CRISPR/Cas9 worm strain generation

The technique described by Dickinson and Goldstein (2016) was used to design and generate a sfGFP-tagged version of TOP-2 (K12D12.1). PCR genotyping was done using the following primers: Genotype-Top2-U1, 5′-GTAAGATTTCCTCTGTAATTTCTTC-3′; and Genotype-Top2-L1, 5′-CCCTAATTTCTACATTTTTCTTCAA-3′.

Worm growth and RNAi experiments

Worm strains N2 (wild type), YPT27 (trt-1[ok410] and XR–VL fusion), TH32(pie-1::bg-1::GFP+unc-119[+]andpie-1::GFP::H2B+unc-119[+]), and OD421 (hcp-3[ok1892] + GFP::HCP-3 + mCherry::H2B) were grown and maintained at 20°C using standard procedures. MDX53 (TOP-2::sfGFP-3×Flag + mCherry::H2B) was grown at 25°C. Bacterial strains containing a vector expressing dsRNA under the IPTG promoter were obtained from the Ahringer library. Targets were confirmed by sequencing. Bacterial strains expressing dsRNAs targeting hcp-3, top-2, and ran-3, as well as the empty vector l4440, were grown overnight, and the cultures were diluted 1:100 and grown at 37°C for 3 h or until reaching OD_{600} between 0.5 and 0.6. For partial depletion, hcp-3 RNAi bacteria were mixed with l4440 RNAi bacterial strain 1:5. For double depletion, the l4440 RNAi bacterial strain was replaced with either the

at half-maximum intensity of individual GFP::CENP-A foci measured on images as in d for control (black; *n* = 21) and csr-1 RNAi (purple; *n* = 18). Box plots were generated with the application found on http://boxplot.tyerslab.com/. Centerlines show the medians. Box limits indicate the 25th and 75th percentiles as determined by R software. Whiskers extend 1.5 times the interquartile range from the 25th and 75th percentiles. *n* = 21 and 18 sample points. (f) Schematic for the model of how CENP-A vs. topo-II impacts chromosome length and the model of centromere expansion vs. neo-centromere formation. Bars, 5 µm. *, P < 0.01.

top-2 or ran-3 bacterial RNAi strain. csr-1, cpar-1, and knl-2 RNAi bacterial strains were grown overnight and used as is. All bacterial RNAi strains were seeded on NGM (nematode growth medium)-IPTG-Carb plates and left to dry overnight. L4 worms were plated on seeded plates and left to grow for 24 h before imaging. To generate dsRNA for injection, 800–900-bp fragments of exons were amplified from genomic DNA using primers 5′-AATTAACCCTCACTAAAGGCCAACGAG TCGATGGTTATG-3′ and 5′-TAATACGACTCACTATAGGTCTCC AACTTGCTCGTATGC-3′ for TOP-2. dsRNA fragments were transcribed in vitro using a High Yield Transcription kit (Ambion). For depletion of topo-II before immunofluorescence, dsRNA was injected into the syncytial gonad of TH32 worms at L4 using an electronic microinjector (Eppendorf) with a needle holder mounted to a microscope (Eclipse TE-2000-S; Nikon).

RNAi screen

N2 and YPT27 worm strains were grown at 20°C to adulthood in NGM liquid culture seeded with OP50 bacteria. Adult worms were bleached to obtain embryos. Embryos were transferred to S basal media and synchronized to the L1 stage. L1 worms were transferred to NGM liquid culture seeded with OP50 bacteria and grown at 20°C for 36 h until L4 stage. L4 worms were cleaned of OP50 bacteria and resuspended in M9 buffer to a mean density of 12–15 worms per 10 µl. A 10-µl drop was deposited, in triplicate, on NGM-IPTG-Carb plates seeded with the bacterial RNAi strain. The RNAi's chosen for the screen were a sublibrary of the whole-genome library and covered the nucleome of *C. elegans* (Tursun et al., 2011). Phenotype was scored 5 d later, and positive results are listed in Fig. 1. All hits were confirmed independently by performing once more the described procedure.

Immunofluorescence

For immunofluorescence, control and RNAi-treated worms were dissected with a scalpel in M9 buffer on a polylysine-coated slide and then placed under a coverslip. Then, the embryos were incubated in liquid nitrogen for 5 min. The coverslip was then removed quickly to break the embryo eggshells, enabling penetration of reagents. Then, embryos were fixed in methanol at −20°C for 30–60 min, washed three times with PBS for 5 min each, and blocked for 30 min with 4% BSA and 0.1% Triton X-100, in PBS. Primary antibodies were incubated at 10 µg/ml for 1.5–2 h and secondary antibodies at 2 µg/ml for 45–60 min. Embryos were washed three times with PBS and three times with PBS–Tween 20, for 5 min each. Embryos were transferred to mounting media containing DAPI for imaging.

Fixed imaging

Fixed-cell imaging was performed on a wide-field epifluorescence microscope (Delta Vision; GE Healthcare) equipped with a camera (CoolSnap HQ2; Photometrics) using a 100× objective (Plan Apo 1.4 NA; Olympus). Softworx imaging software (GE Healthcare) was used for acquisition (with 1 × 1 binning; 0.2-µm z steps) and deconvolution. Imaris software (Bitplane) was used to generate 3D reconstructed images from deconvolved z stacks.

Live imaging

All fluorescence live imaging was performed at RT on a Swept Field confocal microscope (Nikon) mounted on an inverted microscope (TE2000 Eclipse; Nikon) or a confocal microscope (A1R; Nikon) controlled by NIS-elements software (Nikon). Time-lapse acquisitions on the Swept Field microscope were executed using an oil immersion objective (60×/1.4NA PlanApo) at 1.5 magnification and a camera (CoolSnap HQ2). Image acquisition on the confocal microscope (A1R) was executed with a water immersion objective (60×/1.27NA) and a GaASP PMT detector (Nikon) using NIS-elements. *C. elegans* embryos were mounted between a 1.5 coverslip and a microscope slide in M9 buffer on a 5% agarose pad. The coverslip was sealed using Valap (1:1:1 lanolin, petroleum jelly, and parafilm wax). Differential interference contrast imaging was performed on an inverted microscope (te200; Nikon) equipped with an oil objective (100×/1.4NA) and an oil condenser (1.4NA). Images were acquired using an interline charge-coupled device camera (Orca ER; Hamamatsu Photonics) controlled by MetaMorph imaging software (Molecular Devices).

Embryo squashes and chromatin spread

Single-cell embryos were transferred in M9 buffer onto a coverslip for observation on a dissecting microscope. At the desired cell-cycle stage, mounting media was dropped on the embryo, and a microscope slide was used to squash the embryo between the coverslip and the microscope slide. A little bit more pressure was added to the coverslip where the embryo lies to spread the chromatin efficiently.

SIM imaging

SIM imaging was performed on a microscope (Ti-E; Nikon) equipped with an objective (SR Apo TIRF 100×/1.49NA) and an electron-multiplying charge-coupled device detector (iXon3 897; Andor) controlled by NIS-Elements. For each 0.1-µm step, 15 images were acquired (three angles and five phases at each angle). The reconstructed 3D image was use for image processing and analysis.

Image processing, measurements, and analysis

All experiments were repeated at least three times. The number of cells analyzed is stated in the figure legends. Chromosomes lengths were measured as described previously (Ladouceur et al., 2015). In brief, embryos, before NEBD, were visualized in 3D using Imaris (Bitplane), and measurements were made by visually delimiting chromosomes and assigning three points at the extremities and in the middle of individual chromosomes. GFP::HCP-3 and TOP-2::GFP chromatin intensities were measured on maximum intensity projections of embryos after NEBD. Chromosomes were outlined manually to obtain total fluorescence intensities, and the same area of cytoplasmic background was subtracted to obtain the chromatin fluorescence intensities. Each cell was normalized to the highest fluorescence intensity of the individual daily experiment. GFP::HCP-3 intensities per unit length were obtained by segmenting individual chromosomes in 3D using IMARIS software (Bitplane). As in control conditions chromosomes naturally vary in size in individual cells, measurements taken from embryos at the single-cell stage provide sufficient dynamic range. Then, the total GFP intensities were plotted in relation to chromosome length. Chromosomes lengths were sometime measured differently, and therefore the absolute length differs (Fig. 2, manually; Fig. 4, auto-segmentation).

SIM images were analyzed using Fiji. Single foci of GFP::HCP-3 found on stretched chromatin were manually located. A line was drawn across to get the full-width half-maximum using the Plugin FWHM_Line.

TOP-2 graded depletion

TOP-2 was depleted to various extents using dsRNA injection or bacterial feeding for various time periods. To achieve high top-2 depletion (∼95%), 1 mg/ml dsRNA was injected into L4 worms, which were then transferred to TOP-2 dsRNA-expressing bacterial plates and incubated for 2 d at 20°C before imaging. To achieve medium top-2 depletion (∼70%), L4 larvae were incubated on TOP-2 dsRNA-expressing bacterial plates for 2 d at 20°C before imaging. To achieve low top-2 depletion (∼25%), young adults were incubated on TOP-2 dsRNA-expressing bacterial plates for 6.5–8 h at 20°C before imaging.

Depletion levels were quantified by Western blotting using 90 worms (whole-worm lysate) for each condition.

Measuring chromosome axial compaction

For quantitative analysis of chromosome axial compaction, TOP-2 has been depleted to various extents (low ≈ 25% and high ≈ 70%) using RNAi as described in the Worm growth and RNAi experiments section. Lengths of individual horizontally laying chromosomes were measured in each condition just before NEBD using ImageJ software by line scanning.

Online supplemental material

Data concerning the methodological and noncritical aspects of the work are contained in three supplemental figures. This includes measurements referred to in the text and design of the genome-editing approach. Fig. S1 shows. Fig. S2 shows. Fig. S3 shows.

Acknowledgments

The authors would like to thank members of the Maddox laboratories for very helpful discussions and Dr. Dan Dickinson for advice on genome editing and statistical analysis.

A.-M. Ladouceur was supported in part by a dissertation completion fellowship (University of North Carolina at Chapel Hill Graduate School). A.S. Maddox is supported by National Institute of General Medical Sciences grant R01-102390. P.S. Maddox is a William Burwell Harrison Fellow of Biology.

The authors declare no competing financial interests.

Author contributions: A.-M. Ladouceur assisted in conceiving and writing of the study, conducted analysis of chromosome length in various experimental conditions including the screen, and assembled the figures. R. Ranjan constructed the anti–topo-II antibody and performed RNAi analysis as well as immunostaining and constructed Fig. 2. L. Smith participated equally in carrying out and analyzing the RNAi screen. T. Fadero imaged and analyzed the topo-II sfGFP knock-in strain. J. Heppert constructed the topo-II knock-in strain under the guidance of B. Goldstein. A.S. Maddox provided resources including use of microscopes and key intellectual discussion. P.S. Maddox conceived of the study, performed the differential interference contrast on the long-chromosome strain, and wrote the paper.

Submitted: 23 August 2016
Revised: 5 December 2016
Accepted: 19 June 2017

References

Adachi, Y., M. Luke, and U.K. Laemmli. 1991. Chromosome assembly in vitro: Topoisomerase II is required for condensation. *Cell.* 64:137–148. http://dx.doi.org/10.1016/0092-8674(91)90215-K

Belton, J.-M., R.P. McCord, J.H. Gibcus, N. Naumova, Y. Zhan, and J. Dekker. 2012. Hi–C: A comprehensive technique to capture the conformation of genomes. *Methods.* 58:268–276. http://dx.doi.org/10.1016/j.ymeth.2012.05.001

Bembenek, J.N., K.J.C. Verbrugghe, J. Khanikar, G. Csankovszki, and R.C. Chan. 2013. Condensin and the spindle midzone prevent cytokinesis failure induced by chromatin bridges in *C. elegans* embryos. *Curr. Biol.* 23:937–946. http://dx.doi.org/10.1016/j.cub.2013.04.028

Black, B.E., M.A. Brock, S. Bédard, V.L. Woods Jr., and D.W. Cleveland. 2007. An epigenetic mark generated by the incorporation of CENP-A into centromeric nucleosomes. *Proc. Natl. Acad. Sci. USA.* 104:5008–5013. http://dx.doi.org/10.1073/pnas.0700390104

Blower, M.D., B.A. Sullivan, and G.H. Karpen. 2002. Conserved organization of centromeric chromatin in flies and humans. *Dev. Cell.* 2:319–330. http://dx.doi.org/10.1016/S1534-5807(02)00135-1

Buchwitz, B.J., K. Ahmad, L.L. Moore, M.B. Roth, and S. Henikoff. 1999. A histone-H3-like protein in *C. elegans*. *Nature.* 401:547–548. http://dx.doi.org/10.1038/44062

Budirahardja, Y., and P. Gönczy. 2009. Coupling the cell cycle to development. *Development.* 136:2861–2872. http://dx.doi.org/10.1242/dev.021931

Claycomb, J.M., P.J. Batista, K.M. Pang, W. Gu, J.J. Vasale, J.C. van Wolfswinkel, D.A. Chaves, M. Shirayama, S. Mitani, R.F. Ketting, et al. 2009. The Argonaute CSR-1 and its 22G-RNA cofactors are required for holocentric chromosome segregation. *Cell.* 139:123–134. http://dx.doi.org/10.1016/j.cell.2009.09.014

Conklin, E.G. 1912. Cell size and nuclear size. *J. Exp. Zool.* 12:1–98. http://dx.doi.org/10.1002/jez.1400120102

Cuylen, S., C. Blaukopf, A.Z. Politi, T. Müller-Reichert, B. Neumann, I. Poser, J. Ellenberg, A.A. Hyman, and D.W. Gerlich. 2016. Ki-67 acts as a biological surfactant to disperse mitotic chromosomes. *Nature.* 535:308–312. http://dx.doi.org/10.1038/nature18610

De Rop, V., A. Padeganeh, and P.S. Maddox. 2012. CENP-A: the key player behind centromere identity, propagation, and kinetochore assembly. *Chromosoma.* 121:527–538. http://dx.doi.org/10.1007/s00412-012-0386-5

Dickinson, D.J., and B. Goldstein. 2016. CRISPR-based methods for *Caenorhabditis elegans* genome engineering. *Genetics.* 202:885–901. http://dx.doi.org/10.1534/genetics.115.182162

Downes, C.S., D.J. Clarke, A.M. Mullinger, J.F. Giménez-Abián, A.M. Creighton, and R.T. Johnson. 1994. A topoisomerase II-dependent G2 cycle checkpoint in mammalian cells. *Nature.* 372:467–470. http://dx.doi.org/10.1038/372467a0

Eagen, K.P., T.A. Hartl, and R.D. Kornberg. 2015. Stable chromosome condensation revealed by chromosome conformation capture. *Cell.* 163:934–946. http://dx.doi.org/10.1016/j.cell.2015.10.026

Earnshaw, W.C., B. Halligan, C.A. Cooke, M.M. Heck, and L.F. Liu. 1985. Topoisomerase II is a structural component of mitotic chromosome scaffolds. *J. Cell Biol.* 100:1706–1715. http://dx.doi.org/10.1083/jcb.100.5.1706

Farr, C.J., M. Antoniou-Kourounioti, M.L. Mimmack, A. Volkov, and A.C.G. Porter. 2014. The α isoform of topoisomerase II is required for hypercompaction of mitotic chromosomes in human cells. *Nucleic Acids Res.* 42:4414–4426. http://dx.doi.org/10.1093/nar/gku076

Gasser, S.M., T. Laroche, J. Falquet, E. Boy de la Tour, and U.K. Laemmli. 1986. Metaphase chromosome structure: Involvement of topoisomerase II. *J. Mol. Biol.* 188:613–629. http://dx.doi.org/10.1016/S0022-2836(86)80010-9

Gassmann, R., A. Rechtsteiner, K.W. Yuen, A. Muroyama, T. Egelhofer, L. Gaydos, F. Barron, P. Maddox, A. Essex, J. Monen, et al. 2012. An inverse relationship to germline transcription defines centromeric chromatin in *C. elegans*. *Nature.* 484:534–537. http://dx.doi.org/10.1038/nature10973

Geiss, C.P., D. Keramisanou, N. Sekulic, M.P. Scheffer, B.E. Black, and A.S. Frangakis. 2014. CENP-A arrays are more condensed than canonical arrays at low ionic strength. *Biophys. J.* 106:875–882. http://dx.doi.org/10.1016/j.bpj.2014.01.005

Gustafsson, M.G., D.A. Agard, and J.W. Sedat. 1999. I5M: 3D widefield light microscopy with better than 100 nm axial resolution. *J. Microsc.* 195:10–16. http://dx.doi.org/10.1046/j.1365-2818.1999.00576.x

Hara, Y., M. Iwabuchi, K. Ohsumi, and A. Kimura. 2013. Intranuclear DNA density affects chromosome condensation in metazoans. *Mol. Biol. Cell.* 24:2442–2453. http://dx.doi.org/10.1091/mbc.E13-01-0043

Hirano, T., and T.J. Mitchison. 1993. Topoisomerase II does not play a scaffolding role in the organization of mitotic chromosomes assembled in Xenopus egg extracts. *J. Cell Biol.* 120:601–612. http://dx.doi.org/10.1083/jcb.120.3.601

Kieserman, E.K., and R. Heald. 2011. Mitotic chromosome size scaling in Xenopus. *Cell Cycle.* 10:3863–3870. http://dx.doi.org/10.4161/cc.10.22.17975

Ladouceur, A.-M., J.F. Dorn, and P.S. Maddox. 2015. Mitotic chromosome length scales in response to both cell and nuclear size. *J. Cell Biol.* 209:645–652. http://dx.doi.org/10.1083/jcb.201502092

Lowden, M.R., B. Meier, T.W.S. Lee, J. Hall, and S. Ahmed. 2008. End joining at *Caenorhabditis elegans* telomeres. *Genetics.* 180:741–754. http://dx.doi.org/10.1534/genetics.108.089920

Lowden, M.R., S. Flibotte, D.G. Moerman, and S. Ahmed. 2011. DNA synthesis generates terminal duplications that seal end-to-end chromosome fusions. *Science.* 332:468–471. http://dx.doi.org/10.1126/science.1199022

Maddox, P.S., N. Portier, A. Desai, and K. Oegema. 2006. Molecular analysis of mitotic chromosome condensation using a quantitative time-resolved fluorescence microscopy assay. *Proc. Natl. Acad. Sci. USA.* 103:15097–15102. http://dx.doi.org/10.1073/pnas.0606993103

Maddox, P.S., F. Hyndman, J. Monen, K. Oegema, and A. Desai. 2007. Functional genomics identifies a Myb domain-containing protein family required for assembly of CENP-A chromatin. *J. Cell Biol.* 176:757–763. http://dx.doi.org/10.1083/jcb.200701065

Mizuguchi, T., G. Fudenberg, S. Mehta, J.-M. Belton, N. Taneja, H.D. Folco, P. FitzGerald, J. Dekker, L. Mirny, J. Barrowman, and S.I.S. Grewal. 2014. Cohesin-dependent globules and heterochromatin shape 3D genome architecture in *S. pombe*. *Nature.* 516:432–435. http://dx.doi.org/10.1038/nature13833

Mondal, N., and J.D. Parvin. 2001. DNA topoisomerase IIα is required for RNA polymerase II transcription on chromatin templates. *Nature.* 413:435–438. http://dx.doi.org/10.1038/35096590

Monen, J., P.S. Maddox, F. Hyndman, K. Oegema, and A. Desai. 2005. Differential role of CENP-A in the segregation of holocentric *C. elegans* chromosomes during meiosis and mitosis. *Nat. Cell Biol.* 7:1248–1255. http://dx.doi.org/10.1038/ncb1331

Monen, J., N. Hattersley, A. Muroyama, D. Stevens, K. Oegema, and A. Desai. 2015. Separase cleaves the N-Tail of the CENP-A related protein CPAR-1 at the meiosis I metaphase-anaphase transition in *C. elegans*. *PLoS One.* 10:e0125382. http://dx.doi.org/10.1371/journal.pone.0125382

Naumova, N., M. Imakaev, G. Fudenberg, Y. Zhan, B.R. Lajoie, L.A. Mirny, and J. Dekker. 2013. Organization of the mitotic chromosome. *Science.* 342:948–953. http://dx.doi.org/10.1126/science.1236083

Neurohr, G., A. Naegeli, I. Titos, D. Theler, B. Greber, J. Díez, T. Gabaldón, M. Mendoza, and Y. Barral. 2011. A midzone-based ruler adjusts chromosome compaction to anaphase spindle length. *Science.* 332:465–468. http://dx.doi.org/10.1126/science.1201578

Nitiss, J.L. 2009. DNA topoisomerase II and its growing repertoire of biological functions. *Nat. Rev. Cancer.* 9:327–337. http://dx.doi.org/10.1038/nrc2608

Oegema, K., A. Desai, S. Rybina, M. Kirkham, and A.A. Hyman. 2001. Functional analysis of kinetochore assembly in *Caenorhabditis elegans*. *J. Cell Biol.* 153:1209–1226. http://dx.doi.org/10.1083/jcb.153.6.1209

Panchenko, T., T.C. Sorensen, C.L. Woodcock, Z.-Y. Kan, S. Wood, M.G. Resch, K. Luger, S.W. Englander, J.C. Hansen, and B.E. Black. 2011. Replacement of histone H3 with CENP-A directs global nucleosome array condensation and loosening of nucleosome superhelical termini. *Proc. Natl. Acad. Sci. USA.* 108:16588–16593. http://dx.doi.org/10.1073/pnas.1113621108

Rattner, J.B., M.J. Hendzel, C.S. Furbee, M.T. Muller, and D.P. Bazett-Jones. 1996. Topoisomerase II alpha is associated with the mammalian centromere in a cell cycle- and species-specific manner and is required for proper centromere/kinetochore structure. *J. Cell Biol.* 134:1097–1107. http://dx.doi.org/10.1083/jcb.134.5.1097

Schubert, I., and J.L. Oud. 1997. There is an upper limit of chromosome size for normal development of an organism. *Cell.* 88:515–520. http://dx.doi.org/10.1016/S0092-8674(00)81891-7

Steiner, F.A., and S. Henikoff. 2014. Holocentromeres are dispersed point centromeres localized at transcription factor hotspots. *eLife.* 3:e02025. http://dx.doi.org/10.7554/eLife.02025

Taagepera, S., P.N. Rao, F.H. Drake, and G.J. Gorbsky. 1993. DNA topoisomerase II alpha is the major chromosome protein recognized by the mitotic phosphoprotein antibody MPM-2. *Proc. Natl. Acad. Sci. USA.* 90:8407–8411. http://dx.doi.org/10.1073/pnas.90.18.8407

Tursun, B., T. Patel, P. Kratsios, and O. Hobert. 2011. Direct conversion of *C. elegans* germ cells into specific neuron types. *Science.* 331:304–308. http://dx.doi.org/10.1126/science.1199082

Uemura, T., H. Ohkura, Y. Adachi, K. Morino, K. Shiozaki, and M. Yanagida. 1987. DNA topoisomerase II is required for condensation and separation of mitotic chromosomes in S. pombe. *Cell.* 50:917–925. http://dx.doi.org/10.1016/0092-8674(87)90518-6

Warsi, T.H., M.S. Navarro, and J. Bachant. 2008. DNA topoisomerase II is a determinant of the tensile properties of yeast centromeric chromatin and the tension checkpoint. *Mol. Biol. Cell.* 19:4421–4433. http://dx.doi.org/10.1091/mbc.E08-05-0547

Wühr, M., Y. Chen, S. Dumont, A.C. Groen, D.J. Needleman, A. Salic, and T.J. Mitchison. 2008. Evidence for an upper limit to mitotic spindle length. *Curr. Biol.* 18:1256–1261. http://dx.doi.org/10.1016/j.cub.2008.07.092